Biochimica et Biophysica Acta 1854 (2015) 327–332

Contents lists available at ScienceDirect

Biochimica et Biophysica Acta

journal homepage: www.elsevier.com/locate/bbapap

Structural and nanomechanical comparison of epitaxially and solution-grown amyloid β25–35 fibrils

Ünige Murvai [a], Judit Somkuti [a], László Smeller [a], Botond Penke [b], Miklós S.Z. Kellermayer [a,c,*]

[a] Department of Biophysics and Radiation Biology, Semmelweis University, Tűzoltó u. 37-47, Budapest H-1094 Hungary
[b] Supramolecular and Nanostructured Materials Research Group of the Hungarian Academy of Sciences, Dóm tér 8, Szeged, H-6720,Hungary
[c] MTA-SE Molecular Biophysics Research Group, Semmelweis University, Tűzoltó u. 37-47, Budapest, Szeged, Dóm tér 81094 Hungary

ARTICLE INFO

Article history:
Received 29 July 2014
Received in revised form 28 December 2014
Accepted 11 January 2015
Available online 17 January 2015

Keywords:
Amyloid
Atomic force microscopy
Force spectroscopy
Fourier transform infrared spectroscopy
β-Sheet structure
Structural compaction

ABSTRACT

Aβ25–35, the fibril-forming, biologically active toxic fragment of the full-length amyloid β-peptide also forms fibrils on mica by an epitaxial assembly mechanism. Here we investigated, by using atomic force microscopy, nanomechanical manipulation and FTIR spectroscopy, whether the epitaxially grown fibrils display structural and mechanical features similar to the ones evolving under equilibrium conditions in bulk solution. Unlike epitaxially grown fibrils, solution-grown fibrils displayed a heterogeneous morphology and an apparently helical structure. While fibril assembly in solution occurred on a time scale of hours, it appeared within a few minutes on mica surface fibrils. Both types of fibrils showed a similar plateau-like nanomechanical response characterized by the appearance of force staircases. The IR spectra of both fibril types contained an intense peak between 1620 and 1640 cm^{-1}, indicating that β-sheets dominate their structure. A shift in the amide I band towards greater wave numbers in epitaxially assembled fibrils suggests that their structure is less compact than that of solution-grown fibrils. Thus, equilibrium conditions are required for a full structural compaction. Epitaxial Aβ25–35 fibril assembly, while significantly accelerated, may trap the fibrils in less compact configurations. Considering that under *in vivo* conditions the assembly of amyloid fibrils is influenced by the presence of extracellular matrix components, the ultimate fibril structure is likely to be influenced by the features of underlying matrix elements.

1. Introduction

Amyloid fibrils are nanoscale proteinaceous filaments that become deposited, in the form of plaques, in the extracellular space of different tissues in various degenerative disorders [1–3]. The main constituent of amyloid plaques in the brains of patients with Alzheimer's disease are amyloid beta (Aβ) fibrils composed of 39- to 43-residue-long Aβ peptides, which are proteolytic by-products of the transmembrane amyloid precursor protein (APP) [4]. The undecapeptide Aβ25–35 is a naturally occurring proteolytic product of the full-length Aβ [5,6]. It has been proposed that Aβ25–35 represents the biologically active region of Aβ because it is the shortest fragment that exhibits β-sheet-containing aggregated structures and retains the toxicity of the full-length peptide [7]. The peptide, which has a net charge of +1, contains four polar residues at its N-terminus and seven predominantly hydrophobic residues at its C-terminus [8]. The basic features of the Aβ25–35 fibril are similar to those formed from other Aβ peptides. Accordingly, β-strands in an orientation perpendicular to the fibril axis connect to each other via hydrogen bonds and line up to form β-sheet ribbons. The fibril contains several β-sheets that associate *via* amino acid side-chain packing to form the final protofilament structure [9].

Aβ25–35 peptides incubated *in vitro* for an extended period of time (hours to days) form mature amyloid fibrils which are often used as an amyloid model. We have recently shown that the growth of Aβ25–35 amyloid fibrils can be greatly facilitated by an epitaxial mechanism on mica surface. Under these conditions, the peptides form oriented fibrillar network on mica surface within a few minutes [10–12]. Although it has been hypothesized that the epitaxially grown fibrils are identical to the ones evolving under equilibrium conditions in solution, a detailed structural comparison has not yet been carried out. Addressing the structure of epitaxially grown fibrils is compromised by the fact that only a fibrillar monolayer is available for investigation. In the present work we used atomic force microscopy, nanomechanics and FTIR spectroscopy in total internal reflection mode for the structural comparison of Aβ25–35 fibrils grown epitaxially or in bulk solution. We find that although both fibril types are dominated by β-sheet structural elements

Abbreviations: AFM, atomic force microscopy; PBS, phosphate-buffered saline; FTIR, Fourier transform infrared

* Corresponding author at: Department of Biophysics and Radiation Biology, Semmelweis University, Tűzoltó u. 37-47, Budapest H-1094, Hungary.
E-mail address: kellermayer.miklos@med.semmelweis-univ.hu (M.S.Z. Kellermayer).

http://dx.doi.org/10.1016/j.bbapap.2015.01.003
1570-9639/

that display similar nanomechanical properties, the fibrils grown in solution have more compact and polymorphic structure.

2. Materials and methods

2.1. Sample preparation

Aβ25–35 ($^{+}$H3N-GSNKGAIIGLM-COO^{-}) was produced by solid-state synthesis as published earlier [13]. For the study of epitaxially grown fibrils, the peptides were dissolved in dimethyl sulfoxide (DMSO) and transferred to Na-phosphate-buffered saline (Na-PBS) buffer (10 mM Na-phosphate, pH 7.4, 140 mM NaCl, 0.02% NaN_3) at a final concentration of 0.5–1 mg/ml. Insoluble aggregates ("seeds") were removed by centrifugation at 250.000 g and 4 °C for 2 h (Beckman Coulter OptimaTM MAX Ultracentrifuge). The supernatant was diluted to appropriate concentrations prior to further use. According to AFM analysis, the amount of remaining amorphous aggregates was <0.1%. In case of fibrils grown in solution, 0.5–1 mg peptide was dissolved in 10 μl DMSO solution and further diluted with Na-PBS buffer to a final concentration of 0.5–1 mg/ml. The Aβ25–35 fibrils were grown in solution at room temperature for several (typically 2–10) days. The sample was then diluted prior to further investigations. In the case of FTIR experiments, 1 mg/ml Aβ25–35 fibril suspension was concentrated to 25 mg/ml by first vacuum drying in a SpeedVac instrument followed by dissolution of the pellet in D_2O. Two microliters of 25 mg/ml Aβ25–35 samples was used for each measurement. Peptide concentration was measured with the quantitative bicinchoninic acid assay [14].

2.2. Atomic force microscopy

AFM was carried out by steps described in our previous publications [10–12,15–17]. Typically, 100 μl samples were applied to a freshly cleaved mica surface. We used high-grade mica sheets (V2 grade, #52-6, Ted Pella, Inc., Redding, CA). For the study of epitaxially grown fibrils, the seedless sample was incubated for 10 min on the mica surface. In case of fibrils grown in solution, 100 μl of the several-day-old fibrils was pipetted onto freshly cleaved mica surface and then incubated for 30 min. After washing the surface with buffer to remove the unbound fibrils, we scanned the surface with AFM. The samples were imaged with AFM in buffer or in air. Non-contact mode AFM images were acquired with an Asylum Research MFP3D instrument (Santa Barbara, CA) using silicon-nitride cantilevers (Olympus BioLever, resonance frequency in buffer ~ 9 kHz; Olympus AC160 cantilever, resonance frequency in air ~ 330 kHz;). The 512 × 512-pixel images were collected at a typical line-scanning frequency of 0.6–1.5 Hz and with a set point of 0.5–0.8 V.

2.3. Force measurements

Force spectroscopy on Aβ25–35 fibrils was carried out by established protocols [11,12,15–17]. Briefly, a 100 μl sample of Aβ25–35 (8 μM and 950 μM for epitaxially and solution-grown fibrils, respectively) was pipetted on freshly cleaved mica and incubated for 10 min at room temperature. Unbound fibrils were removed by washing gently with buffer (Na-PBS). Surface-bound fibrils were mechanically manipulated by first pressing the cantilever (Olympus BioLever, lever A) tip against the surface, then pulling the cantilever away with a constant, pre-adjusted rate. Typical stretch rate was 500 nm/s. Experiments were carried out under aqueous buffer conditions (Na-PBS buffer, pH 7.4). Stiffness was determined for each cantilever by using the thermal method [18].

2.4. FTIR spectroscopy

The Fourier transform infrared (FTIR) spectra of amyloid fibrils growing in solution were investigated in a diamond anvil cell (Diacell,

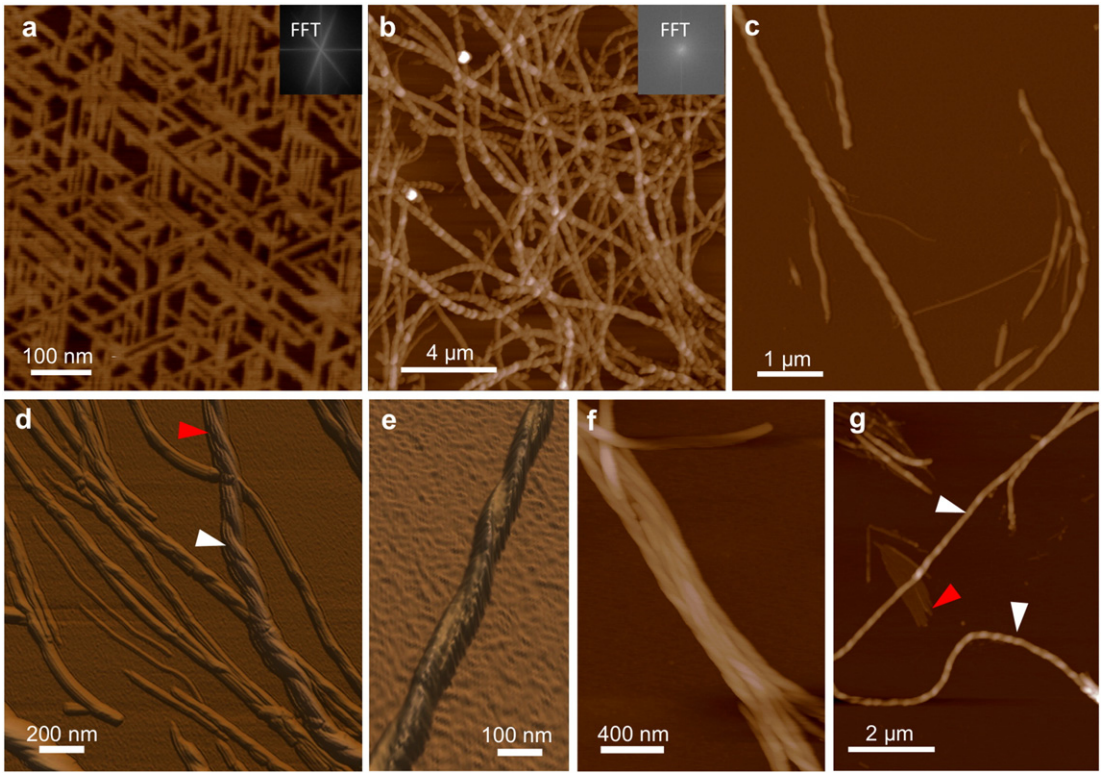

Fig. 1. AFM images showing the morphological appearance of Aβ25–35 fibrils. (a) Epitaxially grown, oriented Aβ25–35 fibril network on mica surface. (b–g) Mature Aβ25–35 fibrils assembled in solution and adsorbed subsequently onto mica. Fibrils display structural polymorphism and different levels of organizational hierarchy: (b) beaded appearance, (c) left-handed helix, (d) fibrils with apparent twist (white arrowhead) and striations (red arrowhead), (e) two fibrils twisted around each other, (f) bundle of twisted fibrils and (g) fibrils with left-handed twist (white arrowheads) and ones showing sheet-like appearance (red arrowhead). Insets, 2D-FFT of the respective AFM image.

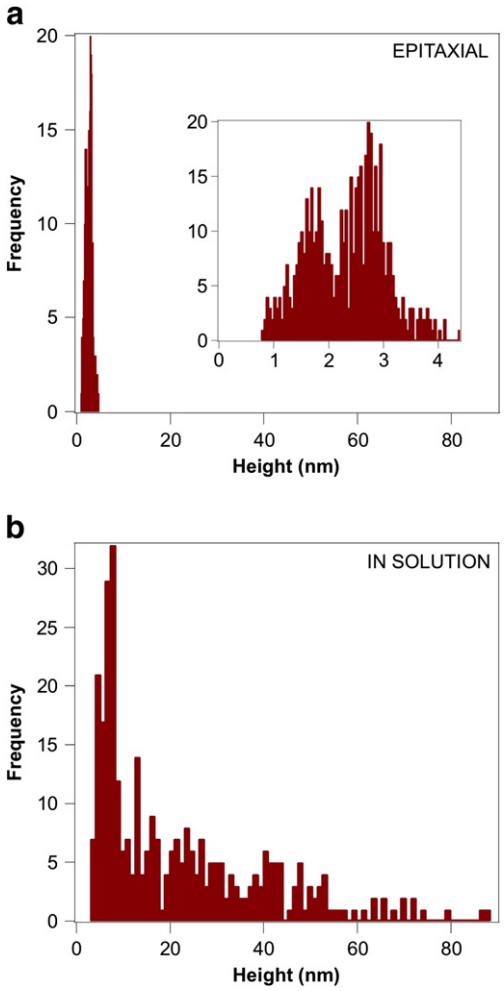

Fig. 2. Topographical height distribution of Aβ25–35 fibrils. (a) Distribution of topographical height of epitaxially grown Aβ25–35 fibrils. Inset shown the distribution within the range of 0–4.5 nm. (b) Distribution of topographical height of solution-grown Aβ25–35 fibrils.

Leicester, UK), which allowed the use of very small sample quantities. To study the secondary structure of epitaxially grown fibrils, 100 μl of 8 μM seedless solution was incubated for 10 min on a freshly cleaved sheet of mica. Unbound fibrils were removed by washing gently with buffer, then the mica surface was dried in N_2 gas. Infrared spectra were recorded by using a Bruker Vertex80v FTIR spectrometer equipped with a high-sensitivity mercury cadmium telluride (MCT) detector. In case of the anvil cell, a beam condenser (Bruker) was used to focus the infrared light on the cell. Two hundred and fifty-six scans were collected at 2 cm^{-1} resolution. Spectral evaluation was performed by using Opus (Bruker) software. The spectra of the mica experiments were corrected for the interference fringes emerging on mica.

2.5. Image processing and data analysis

For data analysis, we used IgorPro v6.0 and ImageJ software. AFM images and force spectra were analyzed with algorithms built in IgorPro v6.03 MFP3D controller software (Wavemetrics, Lake Oswego, OR).

3. Results and discussion

3.1. Topographical structure of Aβ25–35 fibrils

To investigate the structure of Aβ25–35 fibrils and compare the features of epitaxially grown and solution-grown fibrils, we collected topographical images with atomic force microscopy (AFM). Epitaxially grown fibrils displayed a highly ordered trigonal arrangement on freshly cleaved mica surface within a few minutes of incubation (Fig. 1a). As we have previously shown, the formation of oriented fibrils is the result of epitaxial growth rather than the oriented binding of fibrils from solution. The negatively charged mica surface, in a manner similar to phospholipid membranes [19], interacts with Aβ25–35 so that an apparently cooperative interaction between the positively charged ε-amino group of Lys28 and the K^+-binding pocket of the mica lattice determines the oriented binding [10,11]. The trigonal orientation of epitaxially growing Aβ25–35 fibrils is consistent with the hexagonal crystalline lattice structure of the exposed mica surface. The fibrils follow one of the three main directions dictated by the hexagonal array of the surface lattice, although it is not yet known which symmetry framework (i.e., axes crossing the corners *versus* the sides of the hexagons) is preferred. Mica itself lacks direct biological importance and significance. However, because its negatively charged surface binding sites are arranged in a spatially periodic manner (distance between consecutive K^+-binding pockets is 5.2 Å) similarly to biological polymer systems such as collagen or glucosaminoglycans [20–22], the mica-assisted growth of amyloid

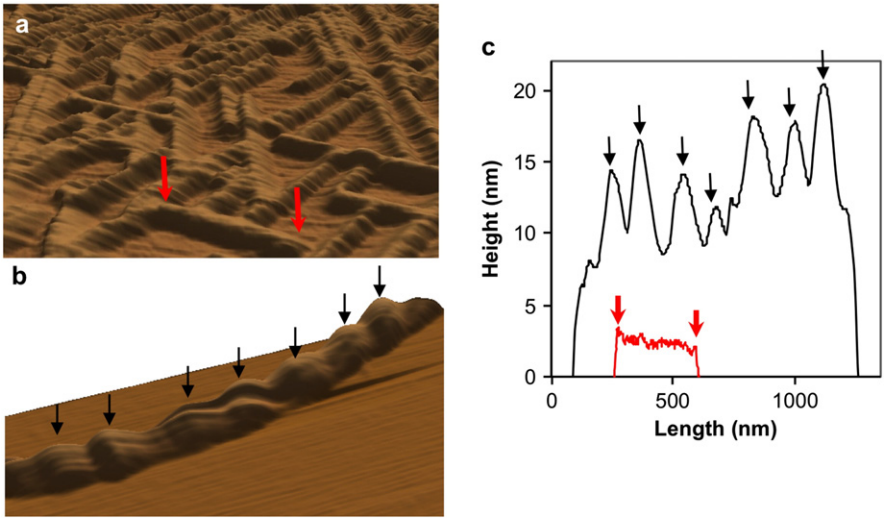

Fig. 3. Axial topography of Aβ25–35 fibrils. (a) AFM image of an epitaxially grown Aβ25–35 fibril selected for analysis, red arrows. (b) AFM image of a solution-grown Aβ25–35 fibril. Arrows highlight the axial periodic structures. (c) Local topographical height of fibrils along the axial contour. Black trace, solution-grown fibrils, red trace, epitaxially grown fibrils. Arrows correspond to the ones in the respective AFM images (a and b).

fibrils may provide clues to the mechanisms of *in vivo* fibrillogenesis facilitated by extracellular matrix components.

To explore the structure of solution-grown Aβ25–35 fibrils, an aliquot of fibrils incubated for several days was applied to mica. A polymorphic, structurally heterogeneous picture emerged (Fig. 1b–g). Some of the fibrils displayed beaded (Fig. 1b) or sheet-like (Fig. 1g) appearance, but most frequently a left-handed helical structure was apparent (Fig. 1c–g). Interestingly, trigonally oriented fibrils were completely absent, indicating that the free Aβ25–35 peptide concentration has, in these samples, already fallen below the critical concentration for epitaxial fibril formation. This observation supports the notion that epitaxially and solution-grown fibrils indeed represent two distinct populations of Aβ25–35 fibrils, which are segregated according to their assembly mechanisms. That is, as long as monomeric Aβ25–35 peptide species are present in large enough solution concentration, the properties of mica dictate the kinetics of fibril formations and the structure of the emerging fibril. If, however, mature fibrils have already formed in solution, the presence of mica does not appear to have a determinant effect on fibril structure. Therefore, the heterogenous ensemble of fibril structures seen in our AFM images likely reflects the variety of equilibrium assembly pathways of Aβ25–35 fibril formation.

To quantitate the structural features of the fibrils, we measured their topographical height distribution (Fig. 2). The range of topographical height was 0.8–4 nm and 7–40 nm for epitaxially ($n = 513$) and solution-grown fibrils ($n = 325$), respectively. As reported previously for epitaxially grown fibrils, the structural unit with 0.8 nm height

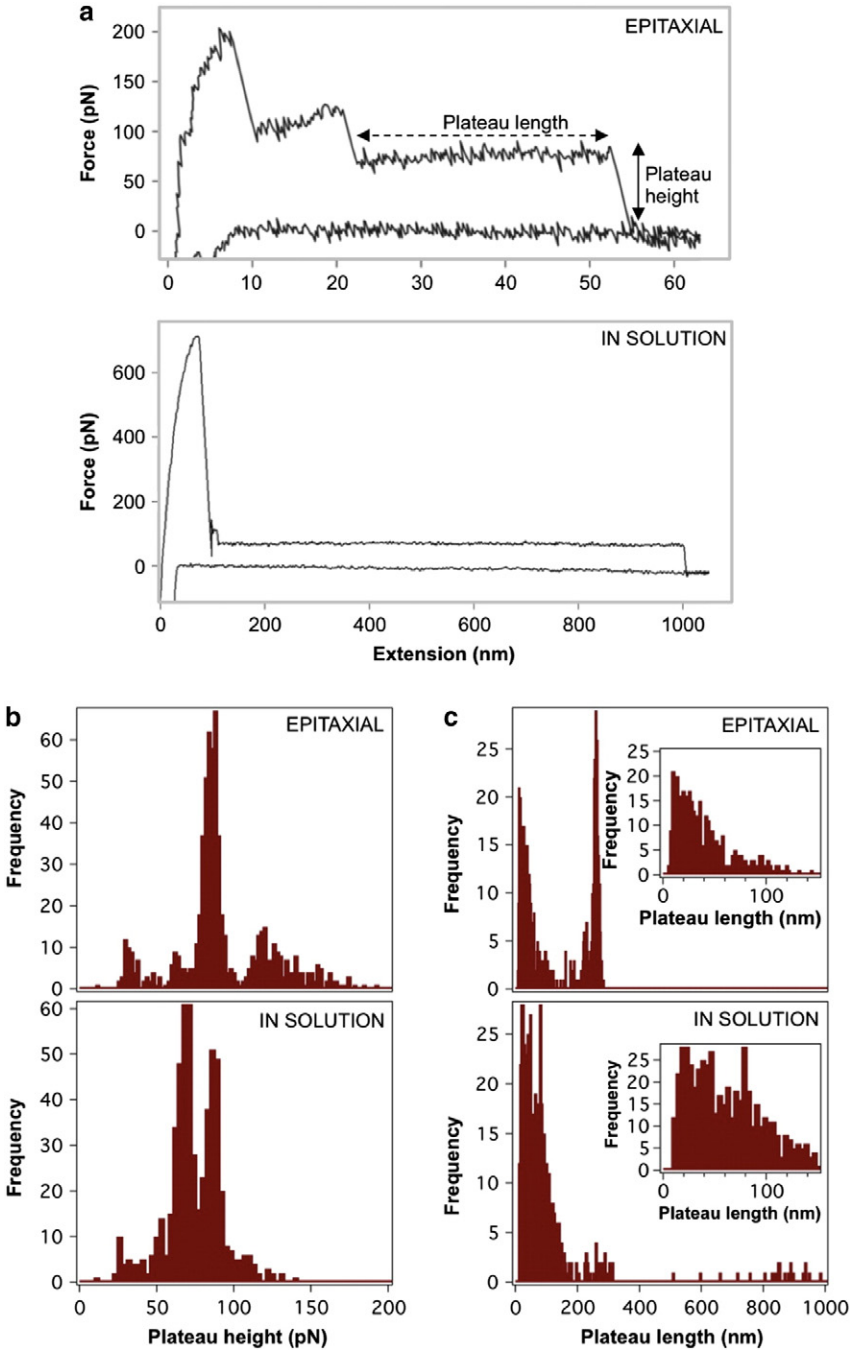

Fig. 4. Nanomechanics of Aβ25–35 fibrils. (a) Representative force curve for an epitaxially grown (top trace) and a solution-grown Aβ25–35 fibril (bottom trace). (b) Distribution of plateau height for epitaxially grown (top graph, number of data points 690) and solution-grown (bottom graph, number of data points 585) Aβ25–35 fibrils. (c) Distribution of plateau length for fibrils grown epitaxially (top graph) and in solution (bottom graph). Insets show the plateau length distributions within the range of 0-150 nm.

most likely corresponds to a single β-sheet [10]. Accordingly, one to five β-sheets build up one epitaxially grown fibril, whereas solution-grown fibrils may contain several tens of β-sheets in parallel.

Epitaxially grown fibrils were significantly shorter than solution-grown fibrils because their length is determined by steric constraints. Whenever the end of an epitaxially growing fibril reaches another fibril on the mica surface, its further growth is halted. Whereas the oriented, epitaxially grown fibrils were only 0.2–3 μm long [10], the length of the fibrils formed in solution, which depends on the free monomer concentration, may reach 10–15 μm.

To reveal further detail about the structural features, we measured the variation of height along the longitudinal axis of Aβ25–35 fibrils. The axial variation of the topographical height was low in the case of epitaxially grown fibrils (Fig. 3a) when compared with that of solution-grown fibrils (Fig. 3b). Solution-grown fibrils most often displayed distinct periodicity related to the underlying left-handed helical structure. The periodicity of these fibrils varied between 50 and 300 nm. Importantly, it took several hours for mature solution-grown fibrils with more-or-less consolidated structures to appear. By contrast, oriented, epitaxially grown fibrils merged within a few minutes after the application of sample onto the mica surface. The acceleration of fibrillogenesis kinetics indicates that mica serves as a catalyzer of Aβ25–35 formation. Within an *in vivo* environment that displays periodically arranged binding sites, such as collagen or glucosaminoglycans [20–22], a similarly catalyzed fibrillogenesis may also be feasible.

3.2. Nanomechanics of Aβ25–35 fibrils

Individual fibrils of either epitaxially or solution-grown Aβ25–35 were mechanically manipulated in order to characterize the intrafibrillar interactions. The nanomechanical behavior of Aβ25–35 fibrils is characterized by the appearance of force plateaus, which correspond to the force-driven unzipping of protofilaments (Fig. 4a) [15–17]. The height of the plateaus is related to the force necessary to unzip the component protofilaments from the underlying fibril driven by the mechanical rupture of the intrafibrillar (i.e., inter-protofilament) interactions (Fig. 4b). Therefore, plateau forces are related to the mechanical stability of the fibril [17]. The higher the plateau, the greater the force necessary to unzip protofilaments and *vice versa*. The length of the force plateau corresponds to the distance between consecutive protofilament rupture events (Fig. 4c). The longer the plateau, the longer it takes for the protofilament to rupture, along its length or at its attachment points, during mechanical unzipping [17]. Thus, plateau length may be loosely correlated with the length of the Aβ25–35 fibrils. The overall appearance of the force spectra was similar for amyloid β25–35 fibrils grown epitaxially or in solution. Both types of fibrils showed plateau-like nanomechanical responses pointing at a similar subfibrillar structure in which protofilaments line up in parallel to form bundles. The fundamental plateau force, defined as the force of the smallest mode within a multimodal distribution [17], was around 30 pN for the epitaxially ($n = 690$) and solution-grown fibrils ($n = 585$) (Fig. 4b). The multimodality of the plateau force histogram is attributed to a coupling between parallel protofilaments within the fibril. Qualitatively similar multimodality is reflected in the topographical height distribution of the fibrils (Fig. 2). Although the plateau length distribution was rather similar for the two fibril types, we sometimes observed very long plateaus in the case of solution-grown fibrils (up to 1000 nm long, Fig. 4c), which are likely due to the unzipping of the entire fibril from the substrate surface [23].

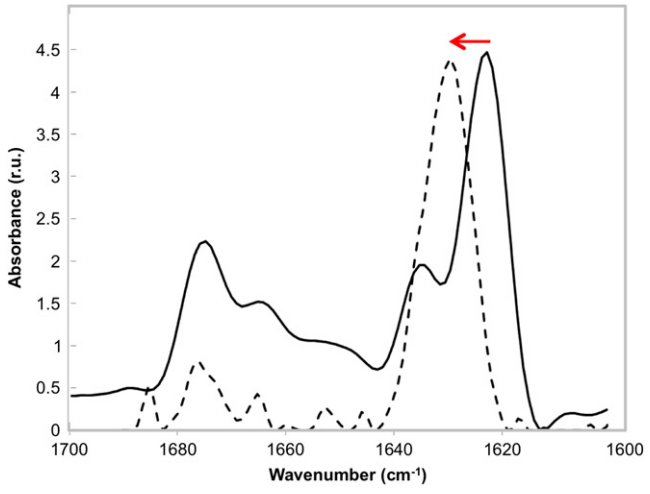

Fig. 5. Deconvoluted FTIR spectra of epitaxially (dashed line) and solution-grown (solid line) Aβ25–35 fibrils. Red arrow indicates the shift of the major peak towards greater wave numbers.

3.3. FTIR spectroscopy

The detailed structural features of the Aβ25–35 fibrils were further explored with Fourier transform infrared (FTIR) spectroscopy. FTIR spectroscopy is frequently used to detect the presence of β-sheet secondary structure and can be adapted for the unconventional arrangement of the surface-adsorbed epitaxially grown Aβ25–35 fibril sample. The approximate position of an IR absorption band is determined by the vibrating masses, the bond type (single, double or triple), the structural location of the electron withdrawing and donating effects of the intra- and intermolecular environment and by coupling with other vibrations [24]. Bands between 1600 and 1700 cm^{-1} are assigned to amide I modes (essentially C = O stretching vibrations of the amide group) and are sensitive to protein secondary structure. As a rule of thumb, a peak near 1645 cm^{-1} is indicative of random coil, 1655 cm^{-1} of α-helix and 1620–1640 cm^{-1} of β-sheet [24–27].

To study the secondary structure of epitaxially grown fibrils, a seedless solution of Aβ25–35 peptides was incubated on a freshly cleaved sheet of mica, which was then investigated in total internal reflection mode. To measure the IR spectrum of solution-grown Aβ25–35 fibrils, a sample incubated for 14 days was used. The IR spectra of the epitaxially and solution-grown fibrils contained an intense peak at 1630 and 1623 cm^{-1}, respectively (Fig. 5). Based on the spectral position of the dominant peak, we conclude that β-sheet elements dominate the structure of both fibril species. A smaller band at 1675 cm^{-1} was also present. Consequently, both types of fibrils are likely to contain anti-parallel β-sheet structures. The assignment of an anti-parallel β-sheet is based on the observation of a peak near 1680 cm^{-1} that arises due to transition dipole coupling and is absent in a parallel β-sheet [28].

Even though both fibril types have similar secondary structures, there are slight differences: the shift in the amide I band from 1623 cm^{-1} in the solution-grown fibrils to 1630 cm^{-1} in the epitaxially grown ones points at a reduced transition dipole coupling and weaker hydrogen bonds in the epitaxial fibrils. These spectral changes reflect the reduced structural compaction of the epitaxial fibrils compared to the ones grown in solution. Conceivably, the oriented arrangement of epitaxially grown fibrils, determined by the interaction between the Lys28 side chains and the K^+-binding pockets of mica, places constraints on the subsequent binding of further Aβ25–35 peptides, thereby resulting in a loosened structure. Thus, while the overall features of epitaxially and solution-grown fibrils are almost identical, the smaller compaction of epitaxially evolved fibrils suggests that interactions with the underlying substrate alter fibril structure.

4. Conclusions

Aβ25–35 fibrils evolve not only in solution conditions but also in an accelerated manner, via epitaxial mechanism, on mica surface. In the present work, we tested whether the fibrils formed under equilibrium conditions are significantly different from those grown epitaxially on the surface. Whereas epitaxially grown fibrils have a uniform

topographical structure characterized by straight fibrils and smooth surface, solution-grown fibrils display considerable polymorphism and structural heterogeneity, curved shape, left-handed helical structure and an axial periodicity ranging between 50 and 300 nm. FTIR spectroscopy revealed that the main structural feature of both fibril types is the β-sheet. Epitaxially grown fibrils are less compact, however, then the ones grown under equilibrium conditions in solution, suggesting that the underlying substrate surface may influence the final structure of the amyloid fibril.

Acknowledgements

This work was supported by grants from the Hungarian Science Foundation (OTKA K84133 and OTKA K109480). The research leading to these results has received funding from the European Union's Seventh Framework Program (FP7/2007-2013) under grant agreement no. HEALTH-F2-2011-278850 (INMiND).

References

[1] J. Hardy, D.J. Selkoe, The amyloid hypothesis of Alzheimer's disease: progress and problems on the road to therapeutics, Science 297 (2002) 353–356.
[2] D.J. Selkoe, Alzheimer's disease: genes, proteins, and therapy, Physiol. Rev. 81 (2001) 741–766.
[3] L.C. Serpell, C.C. Blake, P.E. Fraser, Molecular structure of a fibrillar Alzheimer's A beta fragment, Biochemistry 39 (2000) 13269–13275.
[4] D.J. Selkoe, Images in neuroscience. Alzheimer's disease: from genes to pathogenesis, Am. J. Psychiatry 154 (1997) 1198.
[5] G. Forloni, R. Chiesa, S. Smiroldo, L. Verga, M. Salmona, F. Tagliavini, N. Angeretti, Apoptosis mediated neurotoxicity induced by chronic application of beta amyloid fragment 25-35, Neuroreport 4 (1993) 523–526.
[6] B.A. Yankner, L.K. Duffy, D.A. Kirschner, Neurotrophic and neurotoxic effects of amyloid beta protein: reversal by tachykinin neuropeptides, Science 250 (1990) 279–282.
[7] C.J. Pike, A.J. Walencewicz-Wasserman, J. Kosmoski, D.H. Cribbs, C.G. Glabe, C.W. Cotman, Structure-activity analyses of beta-amyloid peptides: contributions of the beta 25-35 region to aggregation and neurotoxicity, J. Neurochem. 64 (1995) 253–265.
[8] M. van Veen, P. O'Shea, The interaction of the neurodegenerative fragment of the beta-amyloid peptide with phospholipid membranes, Biochem. Soc. Trans. 23 (1995) 547S.
[9] T.R. Jahn, O.S. Makin, K.L. Morris, K.E. Marshall, P. Tian, P. Sikorski, L.C. Serpell, The common architecture of cross-beta amyloid, J. Mol. Biol. 395 (2010) 717–727.
[10] Á. Karsai, L. Grama, Ü. Murvai, K. Soós, B. Penke, M.S. Kellermayer, Potassium-dependent oriented growth of amyloid β25–35 fibrils on mica, Nanotechnology 18 (2007) 345102.
[11] A. Karsai, U. Murvai, K. Soos, B. Penke, M.S. Kellermayer, Oriented epitaxial growth of amyloid fibrils of the N27C mutant beta 25-35 peptide, Eur. Biophys. J. 37 (2008) 1133–1137.
[12] U. Murvai, K. Soos, B. Penke, M.S. Kellermayer, Effect of the beta-sheet-breaker peptide LPFFD on oriented network of amyloid beta25-35 fibrils, J. Mol. Recognit. 24 (2011) 453–460.
[13] M. Zarandi, K. Soos, L. Fulop, Z. Bozso, Z. Datki, G.K. Toth, B. Penke, Synthesis of Abeta [1-42] and its derivatives with improved efficiency, J. Pept. Sci. 13 (2007) 94–99.
[14] P.K. Smith, R.I. Krohn, G.T. Hermanson, A.K. Mallia, F.H. Gartner, M.D. Provenzano, E.K. Fujimoto, N.M. Goeke, B.J. Olson, D.C. Klenk, Measurement of protein using bicinchoninic acid, Anal. Biochem. 150 (1985) 76–85.
[15] A. Karsai, Z. Martonfalvi, A. Nagy, L. Grama, B. Penke, M.S. Kellermayer, Mechanical manipulation of Alzheimer's amyloid beta1-42 fibrils, J. Struct. Biol. 155 (2006) 316–326.
[16] A. Karsai, A. Nagy, A. Kengyel, Z. Martonfalvi, L. Grama, B. Penke, M.S. Kellermayer, Effect of lysine-28 side-chain acetylation on the nanomechanical behavior of alzheimer amyloid beta25-35 fibrils, J. Chem. Inf. Model. 45 (2005) 1641–1646.
[17] M.S. Kellermayer, L. Grama, A. Karsai, A. Nagy, A. Kahn, Z.L. Datki, B. Penke, Reversible mechanical unzipping of amyloid beta-fibrils, J. Biol. Chem. 280 (2005) 8464–8470.
[18] J.L. Hutter, J. Bechhoefer, Calibration of atomic-force microscope tips, Rev. Sci. Instrum. 64 (1993) 1868–1873.
[19] E. Terzi, G. Holzemann, J. Seelig, Alzheimer beta-amyloid peptide 25-35: electrostatic interactions with phospholipid membranes, Biochemistry 33 (1994) 7434–7441.
[20] G. Esposito, A. Corazza, V. Bellotti, Pathological self-aggregation of beta(2)-microglobulin: a challenge for protein biophysics, Subcell. Biochem. 65 (2012) 165–183.
[21] A. Relini, C. Canale, S. De Stefano, R. Rolandi, S. Giorgetti, M. Stoppini, A. Rossi, F. Fogolari, A. Corazza, G. Esposito, A. Gliozzi, V. Bellotti, Collagen plays an active role in the aggregation of beta2-microglobulin under physiopathological conditions of dialysis-related amyloidosis, J. Biol. Chem. 281 (2006) 16521–16529.
[22] A. Relini, S. De Stefano, S. Torrassa, O. Cavalleri, R. Rolandi, A. Gliozzi, S. Giorgetti, S. Raimondi, L. Marchese, L. Verga, A. Rossi, M. Stoppini, V. Bellotti, Heparin strongly enhances the formation of beta2-microglobulin amyloid fibrils in the presence of type I collagen, J. Biol. Chem. 283 (2008) 4912–4920.
[23] Y.L. Lyubchenko, S. Sherman, L.S. Shlyakhtenko, V.N. Uversky, Nanoimaging for protein misfolding and related diseases, J. Cell. Biochem. 99 (2006) 52–70.
[24] A. Barth, Infrared spectroscopy of proteins, Biochim. Biophys. Acta 1767 (2007) 1073–1101.
[25] J.L. Arrondo, A. Muga, J. Castresana, F.M. Goni, Quantitative studies of the structure of proteins in solution by Fourier-transform infrared spectroscopy, Prog. Biophys. Mol. Biol. 59 (1993) 23–56.
[26] Y.N. Chirgadze, B.V. Shestopalov, S.Y. Venyaminov, Intensities and other spectral parameters of infrared amide bands of polypeptides in the beta- and random forms, Biopolymers 12 (1973) 1337–1351.
[27] C.R. Middaugh, H. Mach, J.A. Ryan, G. Sanyal, D.B. Volkin, Infrared spectroscopy, Methods Mol. Biol. 40 (1995) 137–156.
[28] W.H. Moore, S. Krimm, Transition dipole coupling in amide I modes of betapolypeptides, Proc. Natl. Acad. Sci. U. S. A. 72 (1975) 4933–4935.